Available online at www.sciencedirect.com
ScienceDirect
Ceramics International 37 (2011) 2927–2930
CERAMICS INTERNATIONAL
www.elsevier.com/locate/ceramint

Short communication

A comparative study: Hydroxyapatite spherical nanopowders and elongated nanorods

S.K. Swain, D. Sarkar *

Department of Ceramic Engineering, National Institute of Technology, Rourkela, Rourkela 769008, Orissa, India

Received 6 December 2010; received in revised form 18 January 2011; accepted 21 March 2011
Available online 26 May 2011

Abstract

Low temperature wet-chemical method was employed for the synthesis of different grades of hydroxyapatite (HAp) nanoparticles. The elongated nanorods (ENRs) exhibited more crystallinity, higher specific surface area at room temperature but decomposed at low temperature compared to spherical nanopowders (SNPs). Choice of starting precursors and pH of reaction media were the key factors in the formation of these particles. Distinct sintering characteristics and microstructure were noticed because of the difference in thermal stability, pore curing and grain growth.

Keywords: A. Sintering; Hydroxyapatite; Nanopowders; Nanorods; Ceramics

1. Introduction

Synthetic hydroxyapatite (HAp) nanopowder is an imperative source for filler, protein delivery media and scaffolds due to its excellent biocompatibility and bioactivity with the resemblance to the inorganic constituent of bone [1–3]. Nanocrystalline HAp is snugly arranged within collagen fibrils, where collagen, HAp and water supports make bone flexible, rigid and source of interstitial space for nutrients, respectively [4]. The anisotropic mechanical stress distribution with respect to direction has been observed due to the complicated histology of bone. Furthermore, morphology and dimension of intriguing hydroxyapatite nanocrystals have significant effect on mechanical properties, surface chemistry and bioactivity. Therefore, selective morphology of nanometer HAp has an important role in tissue engineering [5]. Extensive synthesis technique of HAp spherical nanopowders and their biomedical application have already been well established. In recent years, the studies on HAp elongated nanorods have also received research attention because of high efficiency as deliver media and scaffolds [6]. Most synthetic apatites are developed via high temperature processes resulting in a well-crystallized structure, which has low bioresorption in contrast to natural apatite. Dalconi et al. depicted that the X-ray diffraction patterns of foetal bone samples are broader than those of adult bone, since younger bones are smaller and/or have more defective crystal structures than adult bones [7]. Hence, understanding on crystallization of synthetic apatite with respect to morphology is an important issue for biomedical use. In this context, different shapes of particles were synthesized and studied for their basic morphological differences in room temperature, crystallinity, thermal stability and sintering behavior for a specific application such as scaffolds.

2. Experimental

2.1. Synthesis of HAp nanopowders and nanorods

Spherical nanopowders (SNPs) was synthesized by co-precipitation method through $Ca(NO_3)_2{\cdot}4H_2O$ and $(NH_4)_2HPO_4$ precursors. Both of the salt solutions were separately prepared by maintaining Ca:P molar ratio 1.67. The $(NH_4)_2HPO_4$ solution was slowly added to the $Ca(NO_3)_2{\cdot}4H_2O$ solution and pH was increased to ~10 with the addition of NH_4OH until entire HAp particles precipitated. The powder was aged for 1 h, washed and dried in oven. In another end, elongated nanorods (ENRs) was synthesized by similar co-precipitation technique through $(CH_3COO)_2Ca$ and KH_2PO_4 as

* Corresponding author. Tel.: +91 661 2462207.
E-mail address: dsarkar@nitrkl.ac.in (D. Sarkar).

0272-8842/$36.00
doi:10.1016/j.ceramint.2011.03.077

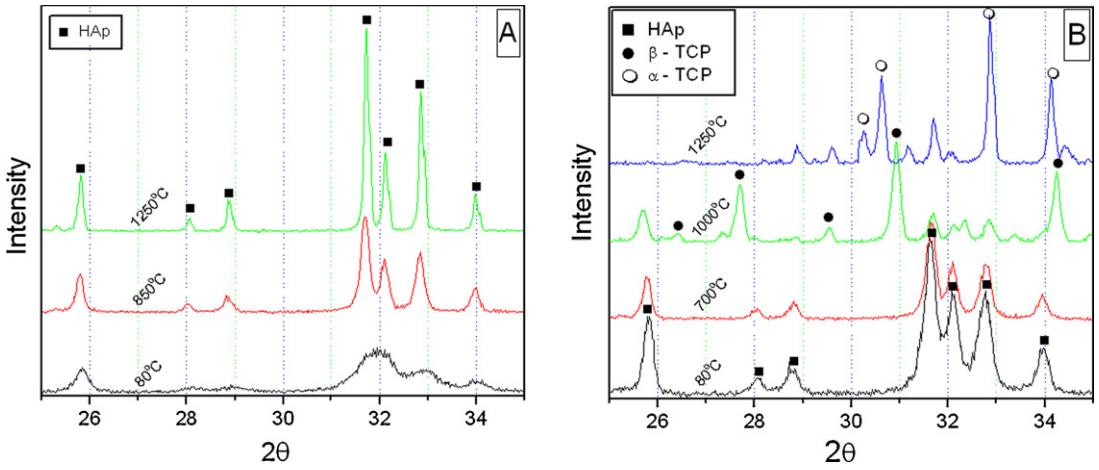

Fig. 1. X-ray diffraction pattern of as-dried and calcined HAp spherical nanopowders (A) and elongated nanorods (B).

starting precursors. Aqueous solutions of $(CH_3COO)_2Ca$ and KH_2PO_4 were prepared with identical molar ratio of calcium and phosphorous atoms in spherical particles. Two solutions were then slowly dropped together within a glass beaker through vigorous stirring. The precipitated HAp was aged for 1 h, washed and oven dried. The basic differences within two processes were the starting precursors and reaction medium, where sphere particles were developed in basic (pH ~10) medium, and rods in weak acidic (pH ~4) condition.

2.2. Characterization of nanoparticles

Phase analysis of Hap nanopowders was studied using the room temperature powder X-ray diffraction (Philips PAN Analytical, Netherlands) with Cu Kα radiation. Samples were scanned in a step scan mode. The presence of functional groups was analyzed by FTIR method (PERKIN ELMER RXI, SPECTRUM, USA) in the scanning range of 4000–400 cm^{-1}. Calcium to phosphate ratio for both of the HAp particles was estimated by chemical analysis. Calcium (Ca) was estimated by complexometric titration with EDTA, whereas phosphorus (P) was estimated by gravimetric method using ammonium molybdate [8]. Specific surface area of powders was taken at nitrogen adsorbate using BET (Quantachrome Autosorb, USA) and particle size was calculated as previous report [9]. Powder morphology and sintered microstructure at different temperatures were elucidated using scanning electron microscope (JEOL JSM 6480LV). The linear shrinkage of green compacts was determined by dilatometer (NETZSH 402, Germany) at a heating rate of 10 °C/min in air. For these measurements, the bar shaped samples of 6 mm × 5 mm × 15 mm were heated up to 1250 °C. Finally, the powders were uniaxially compacted, separately sintered at different temperature profiles for 2 h holding at peak temperature and their microstructure was observed.

3. Results and discussion

Fig. 1A shows the XRD pattern of spherical HAp nanopowder after calcination at different thermal conditions. The pattern of as-dried powder exhibits broad peak of hydroxyapatite phase, which was gradually crystallized at elevated temperatures. High crystalline hexagonal structure: $a = b = 9.4240$, $c = 6.8790$ (JCPDS, 74-0565) of HAp was developed at optimum 850 °C and stable up to 1250 °C. Fig. 1B shows that HAp nanorods are more crystalline at initial condition compared to spherical particles. Beyond 700 °C the HAp nanorods were destabilized and substantially decomposed to β-TCP with other tricalcium phosphate phases. Moreover, the hydroxyapatite phase was decomposed to 90% β-TCP at 1000 °C, but 56% α-TCP, 30% β-TCP and 12% HAp was estimated at 1250 °C. Fig. 2 shows the FTIR spectrum for HAp spherical nanopowders and nanorods. The absorption bands were detected at wave numbers 3436, 1434, 1039, 603, and 554 cm^{-1} for SNPs, whereas 3420, 1031, 603 and 554 cm^{-1} for ENRs. The bands at wave number 1031 and 554 cm^{-1} were associated with the characteristics of PO_4^{-3} group, but bands at 3420 and 603 cm^{-1} represent the characteristic stretching and bending modes for OH^- group, respectively. The absorption

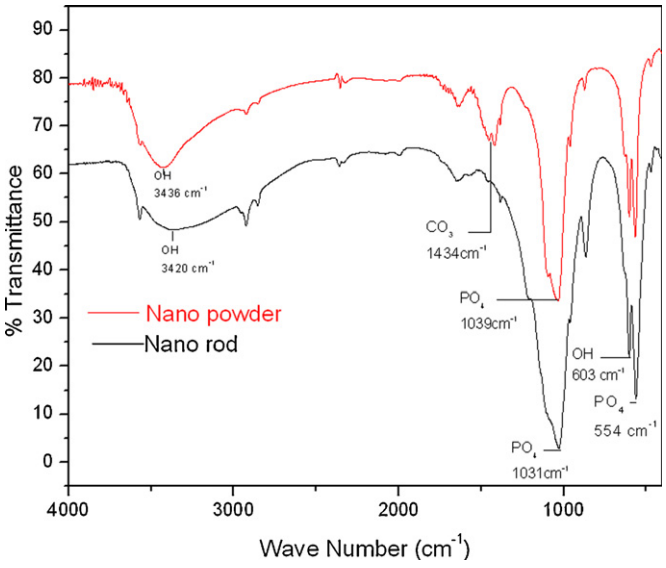

Fig. 2. FTIR spectrum of as-dried HAp spherical nanopowders and elongated nanorods.

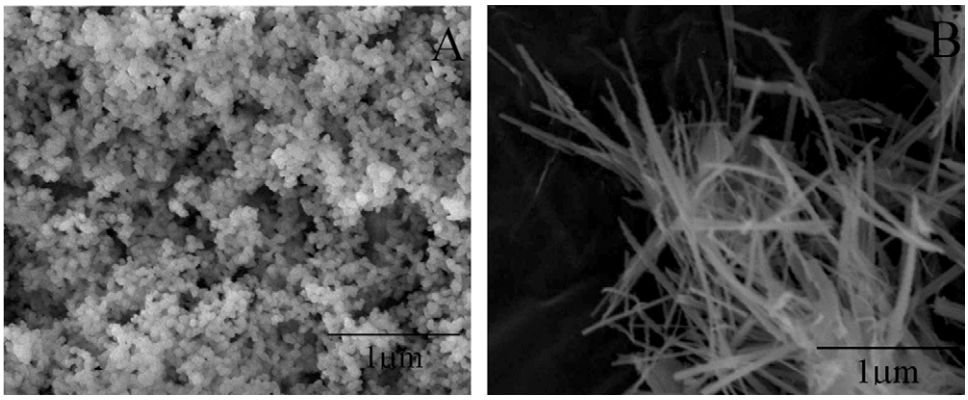

Fig. 3. SEM micrograph of as-dried HAp spherical nanopowders (A) and elongated nanorods (B).

band at 1434 cm^{-1} described the C–O stretching vibration of CO_3^{-2} ions in the spherical HAp nanopowders, which was different from HAp rods [10]. The stretching mode of OH^- in ENRs is broader than SNPs due to the difference in absorbance of moisture during synthesis. Hence, precipitated spherical powders were more carbonated but rods were more prone to the formation of hydroxides. The Ca:P ratio for as-synthesized SNPs and ENRs was calculated as 1.66 and 1.64, respectively. Spherical powders with high Ca/P molar ratio exhibit more thermal stability compared to elongated rods. BET surface area of SNPs and ENRs was estimated as 23.27 m^2/g and 45.33 m^2/g, respectively. Fig. 3A demonstrates that the spherical powders are ∼60 nm as average particle diameter consisting of soft agglomeration. Fig. 3B shows that the HAp nanorods are 50 nm in diameter and average aspect ratio ∼20. The dimension of rod morphology could be controlled by varying the Ca:P ratio, concentration of $(CH_3COO)_2Ca$ and pH of the reaction media [11].

Fig. 4 represents the dilatometric study of both powder and rod after consolidation of green specimens. The dilatometric study of spherical powder shows that the shrinkage started at 750 °C and extended up to 1100 °C, which is attributed to the pore curing, grain growth and solid state sintering of nanoparticles. Nanorod followed two step shrinkage, at first, shrinkage was started in the range at 800–950 °C due to the phase decomposition of HAp to β-TCP and later was associated with α-TCP to β-TCP conversation within 950–1180 °C [12]. The conversion of β-TCP to α-TCP was in the temperature range of 1000–1100 °C and dependent on the shape and size of hydroxyapatite particles [13]. Meanwhile abrupt shrinkage in a narrow temperature difference was observed for HAp nanorods because of grain dissolution and abrupt growth of these particles. Fig. 5 illustrates the sintered microstructure at different temperatures. Low temperature intermediate sintering of spherical powder exhibits more porous structure compared to rods, moreover, the rod shaped morphology gradually disappeared and aspect ratio reduced with increasing temperature. However, at the final stage of sintering condition the rod was less dense with wide range of grain size distribution; this is due to several stages of conversion and decomposition of HAp phase.

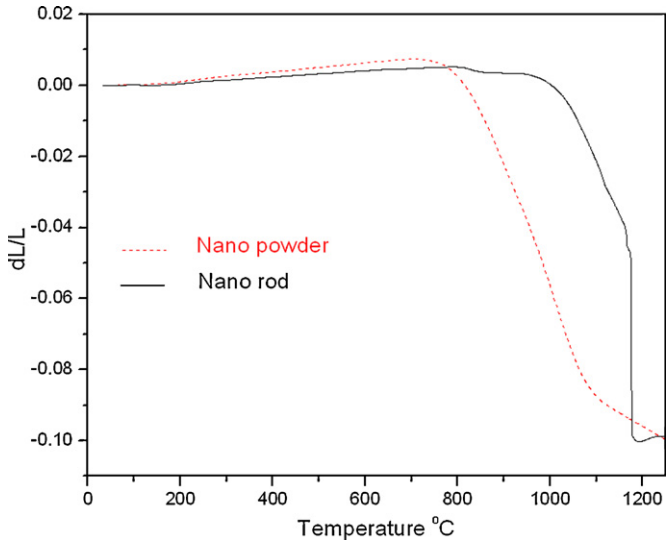

Fig. 4. Linear shrinkage behavior for the green compacts fabricated from HAp nanopowders and nanorods.

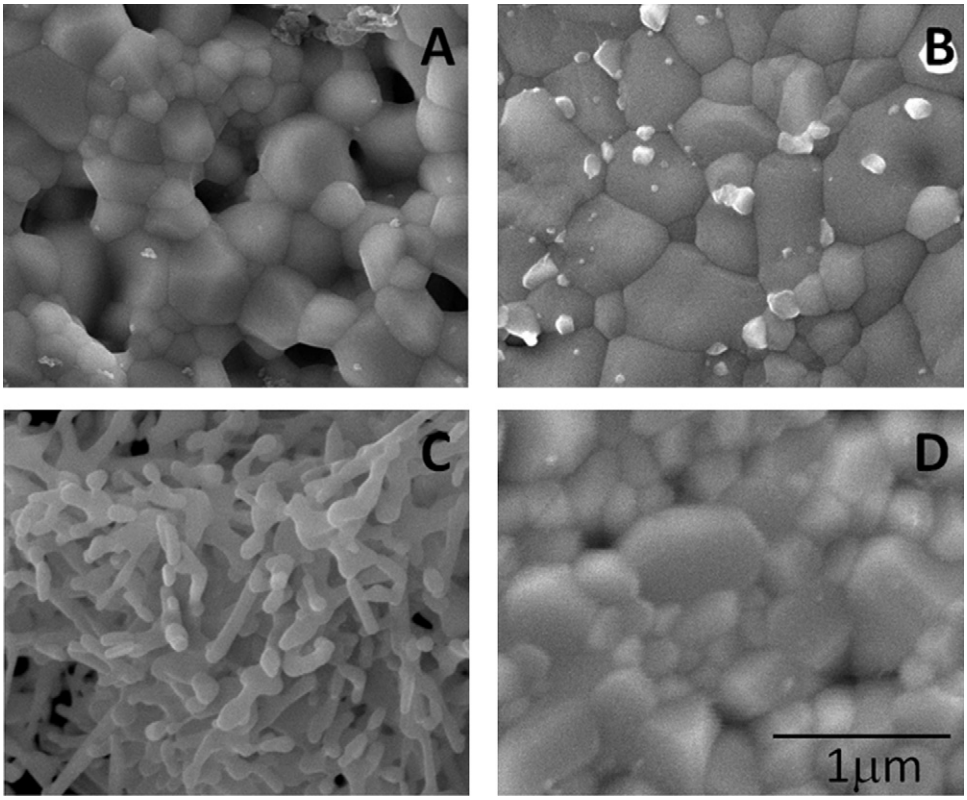

Fig. 5. SEM image of HAp sintered plate: (a) SNPs at 1000 °C, (b) SNPs at 1250 °C, (c) ENRs at 1000 °C and (d) ENRs at 1250 °C.

4. Conclusion

Starting pH is an important parameter to optimize the morphology of hydroxyapatite nanoparticles. The spherical powder has tendency to form carbonated HAp phase. Elongated nanoparticles are thermally less stable, gradually lose their aspect ratio with increasing temperature and develops abnormal grain size distribution when compared to spherical nanopowders.

References

[1] L. Hench, Bioceramics: from concept to clinic, J. Am. Ceram. Soc. 74 (1991) 1487–1510.
[2] H.M. Kim, C. Rey, M.J. Glimcher, Isolation of calcium–phosphate crystals of bone by non-aqueous methods at low temperature, J. Bone Miner. Res. 10 (1995) 1589–1601.
[3] S.K. Swain, S. Bhattachryya, D. Sarkar, Preparation of porous scaffold from indigenous hydroxyapatite powders, Mater. Sci. Eng. C 31 (2011) 1240–1244.
[4] D. Sarkar, M.C. Chu, S.J. Cho, Ceramic–polymer nanocomposite: alternate choice of bone, J. Kor. Ceram. Soc. 45 (2008) 309–319 (Review).
[5] H. Chen, Y. Chen, B.G. Orr, M.B. Holl, I. Majoros, B.H. Clarkson, Nanoscale probing of the enamel nanorod surface using polyamidoamine dendrimers, Langmuir 20 (10) (2004) 4168–4171.
[6] S. Zhang, K.E. Gonsalves, Preparation and characterization of thermally stable nanohydroxyapatite, J. Mater. Sci. Mater. Med. 8 (1997) 25–28.
[7] M.C. Dalconi, C. Meneghini, S. Nuzzo, R. Wenk, S. Mobilio, Structure of Bioapatite in human foetal bones: An X-ray diffraction study, Nucl. Instr. Meth. Phys. Res. B 200 (2003) 406–410.
[8] G.H. Jeffery, J. Bassett, J. Mendham, R.C. Denney, Vogel's Test Book of Quantitative Chemical Analysis, fifth ed., Longman, UK, 1984.
[9] D. Sarkar, D. Mohapatra, S. Roy, S. Bhattacharya, S. Adak, N.K. Mitra, Synthesis and characterization of sol–gel derived ZrO_2 doped Al_2O_3 nanopowder, Ceram. Int. 33 (2007) 1275–1282.
[10] Z.H. Cheng, A. Yasukawa, K. Kandori, T. Ishikawa, FTIR study on incorporation of CO_2 into calcium hydroxyapatite, J. Chem. Soc. Faraday Trans. 94 (1998) 1501–1505.
[11] S. Suzuki, M. Ohgaki, M. Ichiyanagi, M. Ozawa, Preparation of needle-like hydroxyapatite, J. Mater. Sci. Lett. 17 (1998) 381–383.
[12] T.V. Safronova, V.I. Putlyaev, M.A. Shekhirev, Y.D. Tretyakov, A.V. Kuznetsov, A.V. Belyakov, Densification additives for hydroxyapatite ceramics, J. Eur. Ceram. Soc. 29 (2009) 1925–1932.
[13] J.W. Reid, L. Tuck, M. Sayer, K. Fargo, J.A. Hendry, Synthesis and characterization of single-phase silicon-substituted alpha-tricalcium phosphate, Biomaterials 27 (2006) 2916–2925.